Mesoscopic model of hydrogen embrittlement in particle strengthened materials

O. Barrera
School of Engineering, Computing and Mathematics, Oxford Brookes University, UK
Department of Engineering Science, University of Oxford, UK
A.C.F. Cocks
Department of Engineering Science, University of Oxford, UK

Abstract

This work focuses on the constitutive modelling of damage development in particle strengthened materials in the presence of hydrogen. We apply the model to an area at the interface of a dissimilar weld of 8630 steel/IN625 nickel alloy which is known as the 'featureless region'. This region contains an array of M_7C_3 carbides each measuring about $40nm$. Cleavage-like fracture has been observed only in the presence of hydrogen and it is attributed to a combination of two types of hydrogen embrittlement mechanisms: hydrogen-induced decohesion (HID) along the M_7C_3-matrix interface of and a ductile-type fracture (Hydrogen Enhanced Local Plasticity, HELP). Modelling the constitutive behaviour of this region at a continuum level is not appropriate as the major role in the material response is the interaction of the carbide particles with dislocations which is captured at the mesoscopic level. Here we propose a constitutive model of the "featureless zone" that accurately represents the effect of hydrogen on the constitutive response of the M_7C_3 region at the mesoscopic scale. Hydrogen enhances the evolution of dislocations around the M_7C_3 carbides, therefore the stress locally increases affecting the interfacial strength. The result is that, in the region of high hydrogen concentration, the material exhibits softening.

Keywords: Hydrogen embtittement, mesoscopic model, particle strengthened materials, damage evolution, hydrogen diffusion.

Nomenclature

α_1	dimensionless constant
α_2	dimensionless constant
α_3	dimensionless constant
μ_m	Shear modulus of the matrix.
σ_0^H	Initial yield strength of the matrix in the presence of hydrogen.
σ_c	Cohesive strength in presence of hydrogen.
σ_c^0	Cohesive strength in absence of hydrogen.
σ_Y	Yield strength of the matrix.
σ_y^{Lo}	Yield stress due to the prismatic loops.
σ_y^{pore}	Yield stress due to the pores.

σ_y^p Yield stress due to the particles.

C_d Hydrogen concentration at dislocations

C_L Hydrogen concentration at lattice site

C_T Taylor factor

C_T^{trap} Hydrogen concentration at traps

f_p Volumetric fraction of particles.

n_f Fraction of failed interfaces.

r_p radius of carbides

1. Introduction

In this paper we develop a constitutive model for damage development in particle strengthened materials in the presence of hydrogen. In order to provide a physical context we consider the behaviour of dissimilar metal welds material, employed extensively within the offshore oil and gas industries, whose microstructure is highly affected by the presence of carbides-particles. In particular we refer to the region of the interface between a nickel alloy (such as Alloy 625) and a ferritic steel (such as 8630) identified as a 'featureless' region, see Fig. 1a. The microstructure of the featureless region which is about $20\mu m$ wide, contains a distribution of fine M_7C_3 carbides of elliptical shapes with a major axis measuring $40nm$ shown in Fig. 1b. The featureless region can be viewed as a particle strengthened material constituted by a Nickel-based matrix strengthened by the presence of fine carbides. In the presence of hydrogen, this region clearly exhibits a high density of dislocation structures [6] which is in line with hydrogen enhancing dislocation mobility (HELP) as observed experimentally in high strength steels by Robertson [11]. Dislocation structures then form around M_7C_3 carbides which experience an increased state of stress. When the stress experienced by the particles exceeds a critical threshold microcracks will form. Damage of this type develops in a number of particle strengthened composite materials.

Despite the fact that we were unable to observe the formation of microcracks at the interface between the carbides and the matrix in the featureless region, it is generally accepted that hydrogen lowers the cohesive strength of the carbide/matrix interface promoting a decohesion mechanism (HID, Hydrogen Induced Decohesion) [32]. The morphology of the fracture occurs only in the presence of hydrogen and it is attributed to two types of hydrogen embrittlement mechanisms: hydrogen-induced decohesion (HID) along the M_7C_3 interface followed by a ductile-type fracture (Hydrogen Enhanced Local Plasticity). These observations suggest that cracks nucleate at the interface of the M_7C_3 particles due to the high stresses generated locally. Cracks then grow and link with each other through localised, intense, plastic deformation [10].

This phenomenon was previously modeled at a continuum scale by using a cohesive zone modelling type of approach [9]. The model has been initially applied to a single-carbide system. Recently we were able to generate results considering the real microstructure seen in Fig. 1b [10] and [33]. The macroscopic hydrogen diffusion coupled with mechanics has been discussed in [31]. Despite continuum-based models being able to capture some of the essential features, the constitutive behaviour of the carbide-rich area is better described at a mesoscopic level in which the interaction of the particles with dislocation structures developed around the carbides plays the primary role. Moreover, hydrogen atoms move between normal interstitial lattice site (NILS) and trapping sites (dislocations and interfaces), modifying significantly the microstructure. In this case, hydrogen at dislocations affects the evolution of the dislocation structures around the carbides which then reduces the strength of the M_7C_3 /matrix interface.

In the model, we consider two types of hydrogen embrittlement mechanisms: (a) hydrogen-induced decohesion (HID) along the M_7C_3 - matrix interface, i.e hydrogen lowers the cohesive strength of the interface; (b) Hydrogen Enhanced Local Plasticity, i.e. hydrogen promotes the development of dislocation structures at the M_7C_3 carbides. As a consequence the carbides experience a higher level of stress. The net result of

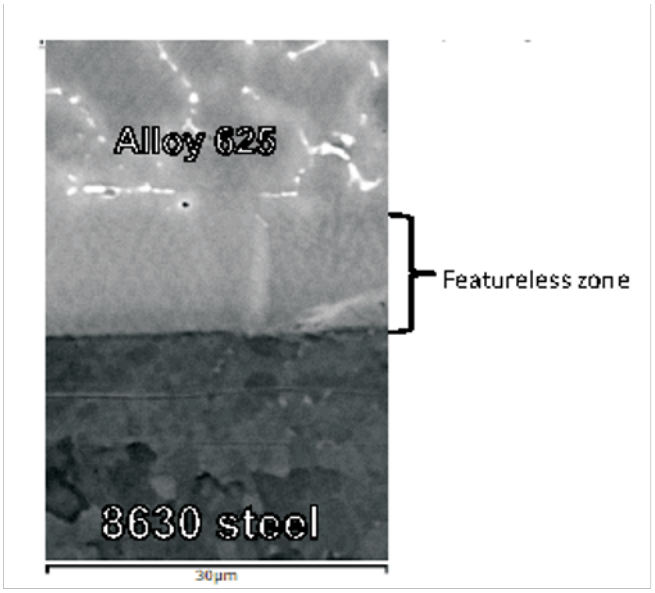

a

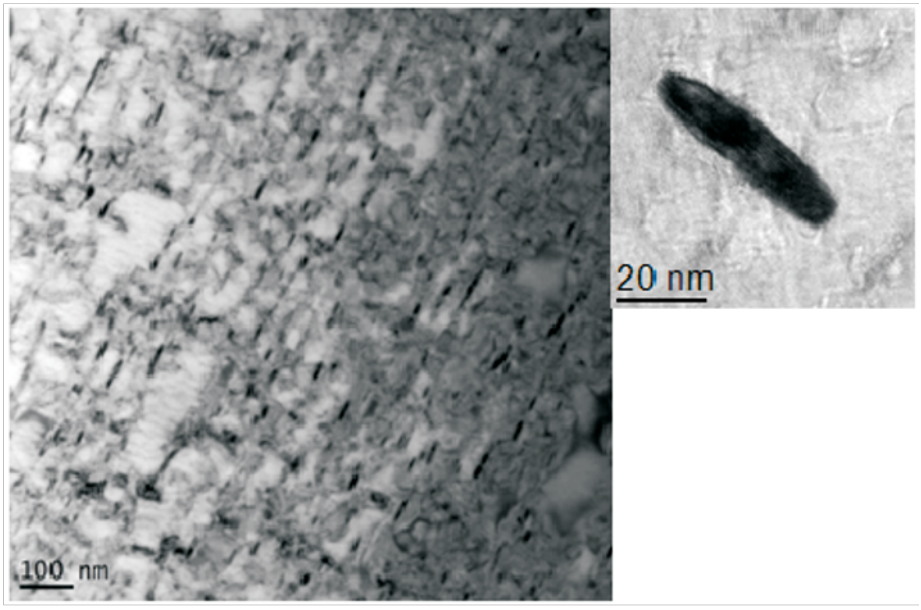

b

Figure 1: (a) An SEM backscatter image showing the featureless zone within an 8630-625 dissimilar weld [5]. (b) Trasmission Electron Microscopy of the carbide-rich region [12]

(a) and (b) is that, in the regions where the concentration of hydrogen is low or absent, the particle matrix interface is intact and the material experience hardening (prismatic dislocation loops that contribute to forrest hardening are punched out from the surface of the particles). In the region where the concentration of hydrogen is significant the material softens as a result of the debonding process at the interface. The model presented here is able to describe hardening and softening in relation to hydrogen diffusion phenomena.

2. A mesoscopic approach to model the M_7C_3 region

Here we propose a model that is capable of reproducing the response of the carbide-rich region in Fig. 1b in the presence of hydrogen. In particular we are interested in developing a mesoscopic model of a representative volume element much larger than the carbide spacing. The particles can either (a) strengthen the material if the interface is intact or (b) weaken the material if the interface fails, the carbides detach from the matrix and are effectively replaced by pores. Particle/matrix failure is dictated by the hydrogen concentration in the bulk that is in equilibrium with the concentration in the traps (carbide-matrix interfaces, grain boundaries and dislocations) and the plastic strain.
Following the physical evidence highlighted in Sec.1, we consider that the plastic behaviour of the carbide rich region is controlled by dislocation glide through a field of dispersed obstacles of M_7C_3 carbides and forest dislocations. The scale of the carbides is such that (1) they interact with discrete dislocations and (2) dislocation structures evolve around the particles. The hydrogen effect in (1) and (2) is extremely important to understand the fracture process in the featureless region. The influence of hydrogen on (1) and (2) affects the plastic properties of the materials, summarized as HELP, where hydrogen facilitates dislocation movement. As a consequence, dislocations pile up at the carbides increasing the stress locally. Moreover (3) the cohesive strength of the carbide/matrix interface degrades with hydrogen content, promoting debonding of the interface. Those failed carbides essentially create micropores. (1), (2) and (3) determine the onset of the softening response.
In [9] the authors discussed the macroscopic response of a volume element containing a single carbide where the cohesive strength of the interface is a function of the hydrogen concentration. The material response lies between that of a body containing a particle with an intact interface and a body containing a pore (interface fails). Initially, the interface is intact, as the material deforms, the stress at the interface increases due to strain hardening of the matrix and the local interaction with punched out dislocations. At the same time the cohesive strength of the interface degrades as a result of the increase in hydrogen concentration. When the stress at the interface reaches the cohesive strength, cracks form and gradually propagate around the interface. The macroscopic response evolves towards that of a porous material. During the debonding process the strengthening due to the carbides is lost. However, the pores created impede dislocation motion and contribute to the yield strength of the matrix, albeit at a lower level than provided by the particles they replace. The debonding of the interface also reduces the rate of hardening in the matrix and the net effect is the softening of the material as observed at a continuum scale [10].

2.1. The effect of hydrogen and plastic strain on the yield strength of the "featureless region"

The Orowan bowing stress governs the initial yield strength of a material strengthened by the presence of particles ([13]). When the material is subjected to plastic deformation, Orowan loops are firstly created around the particles. After one or two loops are formed, punching out of vacancy and interstitial prismatic loops from the particles [13] accommodate the bypass process. The number of prismatic loops N increases proportionally with plastic strain. The material experiences strain hardening when these loops collide with gliding dislocations on other slip planes. We can describe the Orowan bowing stress as [7]:

$$\sigma_y^p = C_T \alpha_1(C_d) \mu b / L_p \tag{1}$$

where C_T is the Taylor factor (approximately equal to 3), μ is the shear modulus, b is the Burger's vector and $L_p = L - 2r_p$ is the spacing between two carbides. L is the separation of pinning centres and r_p is the radius of a carbide particle. If the material contains a volume fraction of randomly arranged carbides f_p,

the mean spacing is $L = 2r_p f_p^{-\frac{1}{2}}$. It is possible to express Eq. 1 as follows:

$$\sigma_y^p = \frac{C_T \alpha_1(C_d) \mu b}{2r_p \left(f_p^{-\frac{1}{2}} - 1 \right)} \tag{2}$$

Based on the fracture surfaces of hydrogen embrittled steels, Beachem [34] suggested that hydrogen promotes unlocking of dislocations. To explain the effect of hydrogen on dislocation mobility Birnbaum and Sofronis [35] proposed a mechanism in which hydrogen formed an atmosphere around dislocations and other elastic stress centres. The redistribution of the hydrogen atmosphere as the stress fields merge effectively shields the dislocations, reducing the interaction energy between the dislocation and the obstacles. The effect of hydrogen is essentially to reduce the applied stress necessary to move an edge dislocation with a hydrogen atmosphere through a field of elastic obstacles. In the present model the presence of hydrogen results in a reduction of dislocation energy i.e. it is easier for a dislocation to bypass the carbides. This results in a reduction of the Orowan bowing stress that we model by considering that $\alpha_1(C_d)$ in eq. 2 is a parameter which decreases with increasing concentration of hydrogen at the dislocations C_d:

$$\alpha_1(C_d) = \alpha_1[C_d(\xi - 1) + 1] \tag{3}$$

α_1 is a dimensionless constant and $\xi = 0.1$ is a softening parameter.

During the deformation process an increasingly dense array of forest dislocations accumulate to accommodate the gradients of deformation. Forest dislocations contribute to obstruct the motion of other moving dislocations resulting in hardening of the material. The total dislocation density is the sum of the geometric necessary dislocation ρ^G and statistical dislocation ρ^S. ρ^S is a characteristic of the material related to its crystal structure, shear modulus, stacking-fault energy etc. ρ^G is a characteristic of the microstructure i.e. geometric arrangement and size of grains and phases. The two populations of dislocation may interact in such a way that ρ^G influences ρ^S but we neglect this phenomenon here. The flow stress depends on the total dislocation density $\rho = \rho^S + \rho^G$. However the increase of the geometrically necessary dislocations ρ^G dominates the development of the dislocation structure at small strain, hence in the following we neglect any changes in ρ^S. The primary source of geometrically necessary dislocation in particle strengthen materials is the prismatic loops punched out from the particles as the material deforms plastically [13], [30]. Consider a body that contains a random array of precipitate particles. Now consider a family of parallel slip planes. The number of particles per unit area of these planes is $\frac{f_p}{\pi r_p^2}$. If dislocations sweep out an area dA on these slip planes in unit volume of material, the body experiences an increment of plastic strain:

$$d\gamma^p = b dA \tag{4}$$

In the process $dA \frac{f_p}{\pi r_p^2}$ particles are bypassed by Orowan bowing, with 4 prismatic loops of radius r_p punched out at each particle. These geometrically necessary dislocation contribute to the overall increase in dislocation density and to forest hardening:

$$d\rho = d\rho_G = \frac{8 f_p}{r_p} dA \tag{5}$$

Eqns. 4 and 5 can be combined to give a relationship between $d\gamma^p$ and $d\rho$. In practice slip will occur on multiple slip systems in different grains of a poli-crystal. For this reason we employ a macroscopic measure of effective strain ϵ^p and motivated by Eqns. 4 and 5:

$$d\rho = \eta d\epsilon_p \tag{6}$$

where $\eta \propto \frac{f_p}{b r_p}$ is a constant for a given material. The form of eq.6 is consistent with the general description given by Gilman [15]. Here we treat η as a parameter to be determined by fitting experimental data. The contribution to the yield stress due to the punching out of the dislocation loops from the particles during the deformation process can be expressed as follows [14]:

$$\sigma_y^{Lo} = C_T \alpha_2(C_d) b\mu\sqrt{\rho} = C_T \alpha_2(C_d) b\mu\sqrt{\rho_0 + \gamma\epsilon^p} \tag{7}$$

where $\alpha_2(C_d)$ is a material parameter that depends on the hydrogen concentration in a similar manner to eq. 3 and ρ_0 is the initial dislocation density. The strengthening associated with dislocations that glide through a field of dispersed obstacles, such as precipitates and forest dislocations, can be difficult to quantify [16]. If none of the carbides fail, the total yield stress is expressed below [16]:

$$\sigma_y = [(\sigma_y^p)^q + (\sigma_y^{Lo})^q]^{1/q} \tag{8}$$

where q is an exponent between 1 and 2, depending on the details of the hardening processes. Over the past two decades available evidence in the literature has suggested that q is generally closer to 2 for the combination of hardening mechanisms considered here. Here we will consider $q = 2$. Eq. 8 is a function of the concentration of hydrogen at dislocations and plastic strain as seen in Eq. 2 and Eq. 7 respectively. The contribution to the total yield strength due to the presence of the particles, σ_y^p, reduces with increasing hydrogen content (Eq. 2), while the contribution due to the punching out of prismatic loops σ_y^{Lo} increases with plastic strain, hence strongly affecting the hardening response.

2.2. Failure at carbide/matrix interface

It is clear that the the plastic strain and the evolution of the hydrogen concentration at dislocations play important roles in determining the material response. The presence of hydrogen results in a weakening of the carbide/matrix interface promoting debonding at the interface. On the other hand, the increase of plastic strain ϵ^p causes an increase of dislocation structures around carbides which increases the stress normal to the carbides. In the present model decohesion at the carbide/matrix interface occurs when the stress normal to the carbides reaches a critical value σ_f. Following the hydrogen induced decohesion (HID) mechanism, the strength at the interface σ_f decreases with increasing hydrogen content. To calculate the stress normal to the carbides we consider that the dominant contribution to the stress at the particle comes from the closest prismatic dislocation punched out from the particle [13]. If we assume that carbides are distributes randomly and that the loops spread to the mid-point between particles, we can express the stress normal to the particle in the form [9, 7]:

$$\sigma = \alpha_3(C_d)_p^{1/2}\epsilon^p + \sigma_I \tag{9}$$

where $\alpha_3(C_d)$ is a parameter which decreases with increasing concentration of hydrogen as described in Eq. 3:

$$\alpha_3(C_d) = \alpha_3[C_d(\xi - 1) + 1] \tag{10}$$

where α_3 is a dimensionless constant. σ_I represents the maximum principal component of the applied stress. The stress normal to the particles evaluated in Eq. 9 increases with increasing plastic strain during the deformation process. The interface will fail when the stress normal to the particle reaches a critical value σ_f. The presence of hydrogen weakens the carbide/matrix interface hence σ_f decreases with increasing hydrogen content.

$$\sigma = \alpha_3(C_d)\mu f_p^{1/2}\epsilon^p + \sigma_I = \sigma_f(C_d) \tag{11}$$

Eq. 11 shows that, at a given plastic strain , the interfaces that are exposed to a higher hydrogen concentration will be more prone to failure.

Now let us assume that the carbides/matrix interfacial strengths Ψ has a distribution as shown schematically in Fig. 2. $\Psi d\sigma_f$ is the number fraction of interfaces with a strength in the range σ_f to $\sigma_f + d\sigma_f$. It is important to note that when the stress in eq. 9 is infinite, all of the carbides have decohered from the matrix. Therefore:

$$\int_0^\infty \Psi d\sigma_f = 1 \tag{12}$$

If the stress in eq. 9 equals σ_i we can write an expression for the fraction of failed interfaces [7]:

$$n_f = \int_0^{\sigma_i} \Psi d\sigma_f \tag{13}$$

At those locations where the interface fails, the matrix debonds from a carbide and the carbide is effectively replaced by a pore. The effect of the pores to the yield strength is expressed as below [7]:

$$\sigma_y^{pore} = \frac{C_T \alpha_2(C_d) \mu b}{2 r_p f_{pore}^{-\frac{1}{2}}} \tag{14}$$

where α_2 is a parameter which decreases with increasing concentration of hydrogen at dislocations as described in Eq. 3 which is less than unity and $f_{pore} = n_f f_p$ is the volume fraction of pores. When a fraction n_f of the interface fails, only $(1 - n_f)$ is effectively taking part to impeding the dislocations mobility, therefore the input to the yield strength from Orowan bowing is decreased to [7]:

$$\sigma_y^p = \frac{C_T \alpha_1(C_d) \mu b}{2 r_p \left(f^{-\frac{1}{2}} - 1 \right)} \tag{15}$$

where $f = (1 - n_f) f_p$. Moreover, in the process of interface weakening in the presence of hydrogen more carbides detach from the interface, therefore fewer carry on generating dislocation loops which contribute to increase hardening, i.e. σ_y^{Lo} in Eq. 7 decreases. $\sigma_y^{Lo}(\epsilon^p)$ expresses the contribution to the yield strength when no carbide debonding occurs and $\dot{\sigma_y}^{Lo} = \frac{\partial \sigma_y^{Lo}}{\partial \epsilon^p}$ is the rate of strength from particles with intact interfaces. Prismatic loops then contribute to the yield strength as follows:

$$\sigma_y^L = \int_0^{\epsilon_p} \sigma_y \dot{Lo} \, (1 - n_f) \, d\epsilon_p \tag{16}$$

The total yield strength of the material is then given by:

$$\sigma_y = \sqrt{(\sigma_y^p)^2 + (\sigma_y^{pore})^2 + (\sigma_y^L)^2} \tag{17}$$

2.3. Constitutive response of the carbide-rich area

As a consequence of loops being punched out from the precipitate and increasing the stress on the particles, the stress in the matrix that drives dislocation motion is reduced. We can capture this behaviour using a kinematic hardening law:

$$g = \sigma_e(\sigma_{ij} - \alpha_{ij}) - \sigma_y = 0 \tag{18}$$

where the yield stress $\sigma_y = \sigma_y(\epsilon_p, n_f, C_d)$ is a function of plastic strain ϵ_p, the fraction of failed particles n_f and concentration of hydrogen trapped at the dislocations C_d. $\alpha_{ij} = (\epsilon_p, n_f)$ is a second order tensor which is a function of plastic strain and volume fraction of unfailed particles $f = (1 - n_f) f_p$ [18, 19, 30] that can be expressed as follows:

$$\alpha_{ij} = 2\eta\mu f \epsilon_{ij}^p = 2\eta\mu(1 - n_f) f_p \epsilon_{ij}^p \tag{19}$$

where η is an accommodation factor that has been tabulated for obstacles of different shape in [19]. The relation in Eq. 18 is related to the work hardening due to internal stresses in the matrix of dispersion hardened materials. In the case where a large fraction of carbides has failed the applied load will be essentially carried by the matrix. The consistency condition states that during plastic deformation the stress must remain on the yield surface. Therefore:

$$dg = \frac{\partial g}{\partial \sigma_{ij}} d\sigma_{ij} + \frac{\partial g}{\partial \alpha_{ij}} \frac{\partial \alpha_{ij}}{\partial \epsilon_{kl}^p} d\epsilon_{kl}^p + \frac{\partial g}{\partial \alpha_{ij}} \frac{\partial \alpha_{ij}}{\partial n_f} dn_f - d\sigma_y = 0 \tag{20}$$

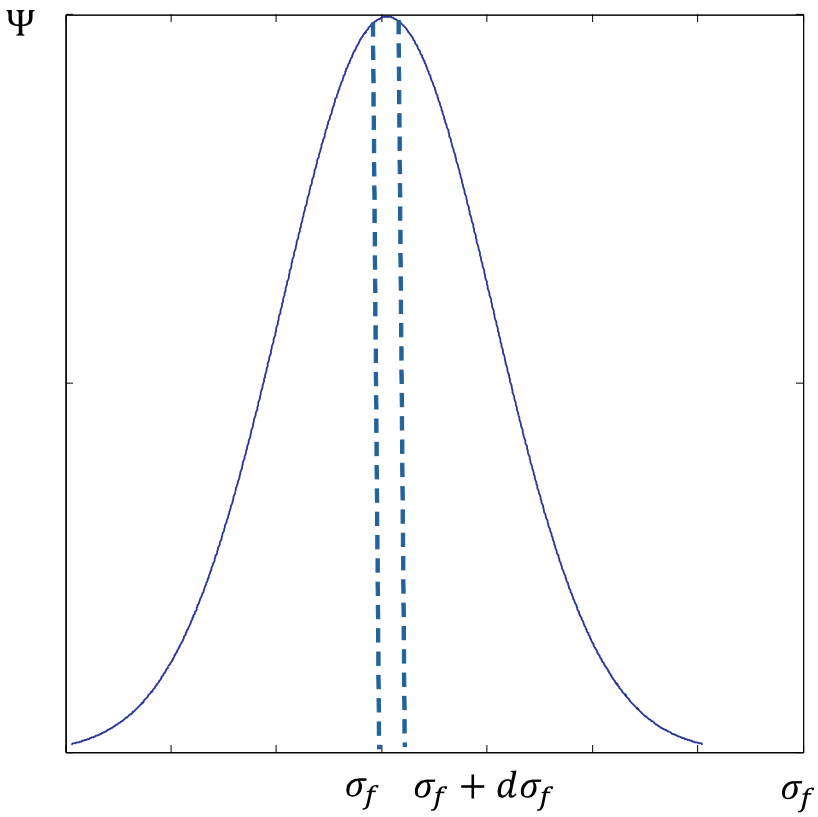

Figure 2: Distribution of the strength of the carbide/matrix interface. [7].

.

where:

$$\frac{\partial g}{\partial \sigma_{ij}} = \frac{\partial \sigma_e}{\partial(\sigma_{ij}-\alpha_{ij})}\frac{\partial(\sigma_{ij}-\alpha_{ij})}{\partial \sigma_{ij}} = \frac{\partial \sigma_e}{\partial(\sigma_{ij}-\alpha_{ij})}$$
$$\frac{\partial g}{\partial \alpha_{ij}} = \frac{\partial \sigma_e}{\partial(\sigma_{ij}-\alpha_{ij})}\frac{\partial(\sigma_{ij}-\alpha_{ij})}{\partial \alpha_{ij}} = -\frac{\partial \sigma_e}{\partial(\sigma_{ij}-\alpha_{ij})} = -\frac{\partial g}{\partial \sigma_{ij}} \tag{21}$$

We assume associated flow, such that $d\epsilon^p_{ij} = \lambda \frac{\partial g}{\partial \sigma_{ij}} = d\epsilon^p_e \frac{\partial g}{\partial \sigma_{ij}}$, where λ is the plastic multiplier. Substituting Eq. 21 into Eq. 20 we obtain:

$$dg = \frac{\partial g}{\partial \sigma_{ij}} d\sigma_{ij} - \frac{\partial g}{\partial \sigma_{ij}}\frac{\partial \alpha_{ij}}{\partial \epsilon^p_{kl}} d\epsilon^p_e \frac{\partial g}{\partial \sigma_{kl}} - \frac{\partial g}{\partial \sigma_{ij}}\frac{\partial \alpha_{ij}}{\partial n_f} dn_f - d\sigma_y = 0 \tag{22}$$

Now considering that $\sigma_y = \sigma_y(\epsilon^p_e, n_f, C_d)$:

$$d\sigma_y = \frac{\partial \sigma_y}{\partial \epsilon^p_e} d\epsilon^p_e + \frac{\partial \sigma_y}{\partial n_f} dn_f + \frac{\partial \sigma_y}{\partial C_d} dC_d \tag{23}$$

Combining eq. 22 and eq. 23 we can write:

$$d\epsilon^p_e = \frac{\frac{\partial g}{\partial \sigma_{ij}} d\sigma_{ij} - \left(\frac{\partial g}{\partial \sigma_{ij}}\frac{\partial \alpha_{ij}}{\partial n_f} + \frac{\partial \sigma_y}{\partial n_f}\right) dn_f - \frac{\partial \sigma_y}{\partial C_d} dC_d}{\frac{\partial \sigma_y}{\partial \epsilon^p_e} + \frac{\partial g}{\partial \sigma_{ij}}\frac{\partial \alpha_{ij}}{\partial \epsilon^p_{kl}}\frac{\partial g}{\partial \sigma_{kl}}} \tag{24}$$

With the individual components of strain given by:

$$d\epsilon^p_{ij} = \frac{\frac{\partial g}{\partial \sigma_{mn}} d\sigma_{mn} - \left(\frac{\partial g}{\partial \sigma_{mn}}\frac{\partial \alpha_{mn}}{\partial n_f} + \frac{\partial \sigma_y}{\partial n_f}\right) dn_f - \frac{\partial \sigma_y}{\partial C_d} dC_d}{\frac{\partial \sigma_y}{\partial \epsilon^p_e} + \frac{\partial g}{\partial \sigma_{pq}}\frac{\partial \alpha_{pq}}{\partial \epsilon^p_{kl}}\frac{\partial g}{\partial \sigma_{kl}}} \frac{\partial g}{\partial \sigma_{ij}} \tag{25}$$

In this section we have presented the constitutive equations as functions of the concentration of hydrogen at the dislocations C_d which is determined locally by the diffusion of hydrogen within the bulk. In the next section we present an appropriate diffusion model which considers the coupling of diffusion and inelastic deformation.

3. Hydrogen diffusion equation and its effect on plasticity

Hydrogen diffuses easily through metals leading to embrittlement even at low concentration [32]. Atoms of hydrogen are located at normal interstitial sites (NILS) or trapping sites: vacancies, defects, interfaces dislocations. Transport phenomena of hydrogen are highly affected by trapping sites since the presence of even weak traps can have a significant effect on the diffusivity. It is common to distinguish between two populations of hydrogen: Hydrogen in the lattice (or in the bulk) which we denote as C_L and hydrogen in traps denoted by C_T^{trap}. While the concentration of hydrogen in the bulk scales linearly with the fraction of NILS sites, hydrogen concentration in traps has a non linear dependency on the fraction of the trap population, hence models of hydrogen transport have been proposed which takes this into account.

One of the first theories on the mobility was given by McNabb and Foster [20] who introduced a diffusion equation of hydrogen in an iron lattice including the effect of trapping sites through the addition of sources and sinks terms. The theory was reformulated and simplified by Oriani [21] in which an important assumption of local equilibrium between the two hydrogen populations (in the case of a low degree of trap coverage) was introduced. The model of Oriani then formed the basis for modelling transport phenomena of hydrogen coupled with large deformation and plasticity [22]. In [22] it was demonstrated that the

concentration gradient, hydrostatic stress and the presence of trapping sites determines the diffusion process. The assumption is that hydrogen atoms move through lattice sites and are trapped at interfaces (such as particle/matrix) and defects/dislocations. During the deformation process, particle/matrix interfaces and dislocations generated by plastic deformation evolve and influence the diffusion process. The transport model proposed in [22] was then modified by Krom et al. [23] by including a factor depending on the strain rate which allows for hydrogen concentration in lattice sites to decrease due to the filling of trap sites.
We use here the hydrogen diffusion equation given in [23]. We consider three types of traps: dislocations , grain boundaries , carbide/matrix interfaces, identified by the symbols d, gb and c respectively. The concentration in the traps C_T^{trap} is related to the density of traps N_T:

$$\frac{D}{D_{eff}}\frac{dC_L}{dt} = \overrightarrow{\nabla}(D\overrightarrow{\nabla}C_L) - \overrightarrow{\nabla}(\frac{DV_H}{3RT}C_L\overrightarrow{\nabla}\sigma_h) - \alpha^d\theta_T^d\frac{\partial N_T^d}{\partial\epsilon^p}\frac{\partial\epsilon^p}{\partial t} \tag{26}$$

Oriani's theory [21] provides a relationship between the diffusivity of the bulk, D, the effective diffusivity of a material with a distribution of traps and the gradient of the concentration in the traps with respect to the bulk concentration:

$$\frac{D}{D_{eff}} = 1 + \sum_{trap}\frac{\partial C_T^{trap}}{\partial C_L} \tag{27}$$

V_H is the partial volume of hydrogen in solid solution and σ_h the hydrostatic stress. The concentrations in the bulk C_L and the traps C_T^{trap} are related to the number of sites occupied by the hydrogen atoms. The concentration in the bulk C_L is related to the number of lattice sites per unit volume N_L:

$$\mathrm{C}_L = \beta\theta_L\ \mathrm{N}_L \tag{28}$$

where $N_L = \frac{N_A\delta}{A_r}atoms/m^3$, N_A is Avogadro's number=$6.022\times10^{23}atoms/mol$ and β is the number of interstitial sites per atom, $\theta_L = \in [0,1]$ is the fraction of trapping sites occupied by H atoms. δ is the density of the metal which is $8.44\times10^3kg/m^3$ at 293 K for Nickel. A_r is the atomic weight of atoms in the host lattice which is $58.7\times10^{-3}kgmol^{-1}$ for Nickel. Hence $N_L = 8.46\times10^{28}atoms/m^3$. The concentration of hydrogen in a given type of trap is given by:

$$C_T^{trap} = \theta_T^{trap}\alpha^{trap}N_T^{trap} \tag{29}$$

where θ_T^{trap} is the trapping site occupancy i.e. θ_T^d (dislocations), θ_T^{gb} (grain boundaries), θ_T^c (carbide-matrix). The trapping site occupancy is always in equilibrium with the lattice site occupancy θ_L (Oriani's theory):

$$\frac{\theta_T^j}{1-\theta_T^j} = \frac{\theta_L}{1-\theta_L}\exp(\frac{W_B^j}{RT}) \tag{30}$$

where the superscript j denotes any of (c, gb, d). α^{trap} denotes the number of sites per trap .
N_T^{trap} indicates the trap density measured in number of traps per unit volume. The trap density can be estimated when only dislocation cores are considered as trap sites [24]. In the trap model it is assumed that only one trap per atomic plane is threaded by a dislocation, that traps are isolated, i.e. they do not form an extended network, and transport between traps occurs by lattice diffusion. The dislocation trap density is expressed as follows [24]:

$$N_T^d = \frac{\sqrt{2}\rho}{a} \tag{31}$$

where a is the lattice constant and ρ is the dislocation density as seen in Eq. 5.
The dislocation density varies from $10^{10}m^{-2}$ in the annealed state to $10^{16}m^{-2}$ in the cold-worked state. More recent development on th influence of microstructural traps on hydrogen diffusion and embrittlement

can be found here [36]. Hence N_T varies between $5 \times 10^{21} m^{-3}$ to $5 \times 10^{27} m^{-3}$. As a result of Eq. 26 the following quantities are evaluated:

C_L: Concentration in the bulk.
C_d: Concentration at dislocations.
C_{gb}: Concentration at grain boundaries.
C_c: Concentration at carbide/matrix interface.
which are all functions of position and time.

4. Numerical results: 1D stress-diffusion problem

The mesoscopic model presented in Sec.2 describes the micromechanical behaviour observed in the featureless region of a dissimilar metal weld (Fig. 1b). The carbide-rich region in Fig. 1b is essentially a Nickel alloy matrix containing M_7C_3 carbides that can either contribute to (a) hardening of the material if the carbides do not decohere from the Ni-alloy matrix or (b) softening of the material if the particles fail and effectively are substituted by pores. The process of failure of carbides is dictated by the hydrogen concentration in the bulk that is in equilibrium with the concentration in the traps (carbide-matrix interfaces, grain boundaries and dislocations) and the plastic strain rate.

In order to illustrate the behaviour of the model, we consider the 1D coupled diffusion-displacement rate control problem shown in Fig. 3. The diffusion equation (Eq. 26) is solved in terms of concentration of hydrogen in the lattice C_L and using Oriani's theory we can evaluate the concentration of hydrogen at the traps : (a) dislocations C_d, (b) grain boundaries C_{gb} and (c) carbide/matrix interfaces C_c. It proves convenient to express the hydrogen concentration in terms of the occupancy, i.e. the number of hydrogen atoms per unit volume normalized with respect to the maximum number of interstitial hydrogen atoms. The occupancy for each type of site varies between $0 - 1$. We consider the situation where the lattice occupancy θ_L is imposed at the boundary (left side of the bar) as shown in Fig. 3 and a no-flux boundary condition at the other end of the bar. A displacement rate is also applied in the direction perpendicular to the bar (Fig. 3), i.e. vertically.

We solve first the hydrogen diffusion equation (Eq. 26). The occupancy in the lattice θ_L is in equilibrium with the occupancy of hydrogen at dislocations θ_T^d. C_{gb} is a function of the trap density at the dislocations N_T^d, which increases with increasing plastic strain as seen in Eq. 31, but θ_T^d is independent of trap density and is related to θ_L through Oriani's relationship of Eq. 30. Since all the occupancies are related to each other through Eq. 31, we can use any one of these to characterise and represent the hydrogen content within the material. Here we choose θ_T^d.

When solving Eq. 26 we use the parameters summarised in Table.1 [27]. The initial hydrogen concentration at x=0 is $C_L = 1 \times 10^{25} atoms/m^3$ which correspond to a value of $\theta_L = 1.97 \times 10^{-5}$. Fig. 4 shows the hydrogen occupancy at dislocations θ_T^d along the bar at different instants of time. If we consider the distribution of hydrogen at dislocations in Fig. 4, it can be seen that (a) the hydrogen content increases during the deformation process and with time and (b) the locations along the bar closer to the source (left and side Fig. 3) are more affected by the hydrogen. C_d decreases as we move away from the source. We consider 6 locations within the domain ranging from $x = 0$ to $x = 1$ as shown in Fig. 3: I at $x = 0$, II, III, IV, V,VI at $x = 1$. Location I which is at $x = 0$ experiences the highest hydrogen content.

Once the occupancy θ_T^d, and hence θ_T^c, is known we can evaluate if the stress normal to the particles exceeds the carbide/matrix interface critical stress σ_f (Eq. 11). σ_f decreases with increasing hydrogen content θ_T^d. Those locations along the bar closest to the source in Fig. 3 experience the higher hydrogen content, hence the interface critical stress decreases more at these locations, resulting in a higher number fraction of failed carbide/matrix interfaces. Here we assume that in the absence of hydrogen $\sigma_f = 1GPa$ and $\sigma_f = 0.4GPa$ when the concentration of hydrogen reaches its maximum value in those locations closest to

Number of trapping sites carbide-matrix interface	$\alpha_c = 9.09 \times 10^{12}$
Number of trapping sites grain boundaries	$\alpha_{gb} = 1$
Number of trapping sites dislocations	$\alpha_d = 1$
Carbide-matrix density	$N_T^c = 5.5 \times 10^{11} m^{-3}$
Grain boundary density	$N_T^{gb} = 10 \times 10^{23} atoms/m^3$
Binding energy of dislocations	$W_B^d = 18kJ/mol$
Binding energy of grain boundaries	$W_B^{gb} = 48kJ/mol$
Binding energy of carbide-matrix interface	$W_B^c = 72kJ/mol$
Lattice site density	$N_L = 8.46 \times 10^{28} atoms/m^3$
Number of interstitial sites per atom	$\beta = 6$
Metal density	$V_M = 7.1110 \times 10^{-6} m^3/mol$
Partial volume of hydrogen in solid solution	$V_H = 2 \times 10^{-6} m^3/mol$
Diffusivity of the bulk	$D = 1.5 \times 10^{-8} m^2/sec$
Lattice parameter	$a = 2.88 \times 10^{-10} m$
Shear modulus	$\mu = 76GPa$
Dimensioneless constants	$\alpha_1 = 1$, $\alpha_2 = 0.3$, $\alpha_3 = 0.1$

Table 1: Parameters used for solving the 1D stress-diffusion problem

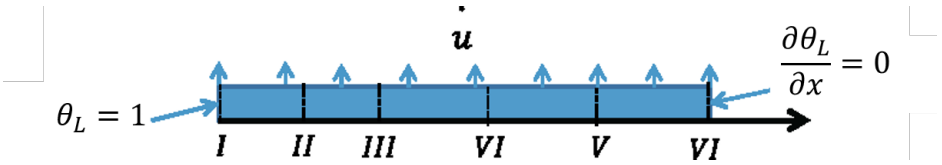

Figure 3: 1D stress-diffusion problem. Locations I, II, III, IV, V, VI are considered when showing how the material behaviour changes in space during the diffusion process.

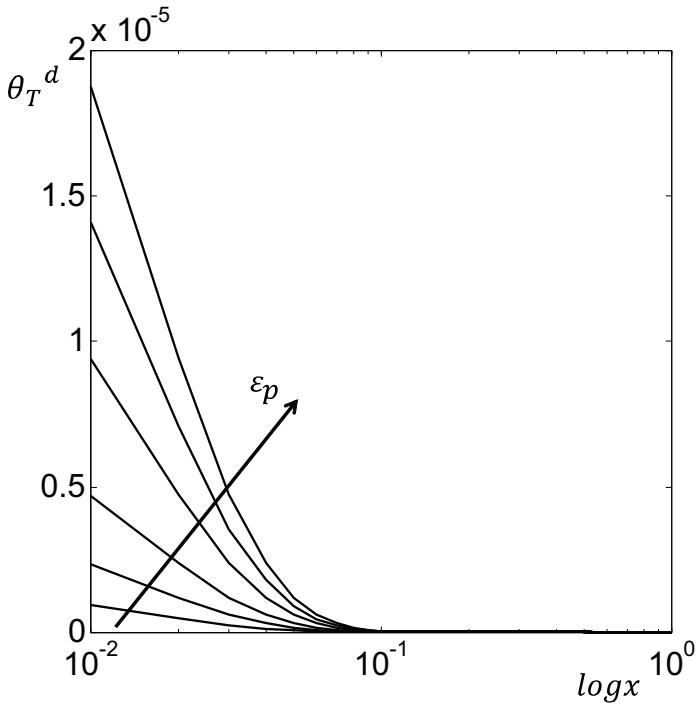

Figure 4: Hydrogen occupancy at dislocation at different instants of time.

the source (left hand side of Fig. 3. The number fraction of failed interfaces n_f is evaluated in Eq. 13 and is function of plastic strain and hydrogen content θ_T^d. The evolution of n_f with plastic strain is shown in Fig. 5 at different locations along the bar where the interface experiences different values of σ_f. The evolution of number fraction of failed particles n_f is bounded between curves I and VI in Figure 5. The hydrogen concentration is zero at x=1. Therefore curve VI corresponds to the situation where the interface failure stress has a constant value $\sigma_f = 1GPa$. At this location the threshold value of plastic strain before any carbide failure occurs is $\epsilon_p = 0.09$ and $n_f = 0.22$ at $\epsilon_p = 0.2$. At location I the traps are almost saturated with hydrogen throughout the deformation process. The interface strength in this limit is $\sigma_f = 0.4GPa$. Here the interface is at its lowest strength. In this case, the threshold value of plastic strain is reduced to $\epsilon_p = 0.03$ and the number fraction of failed particle at the end of the deformation process is $n_f = 0.68$. Based on the consideration above we can extrapolate an expression for $n_f = f(\theta_T^d, \epsilon_p)$ along the bar as follows:

$$n_f(\theta_T^d, \epsilon_p) = [2(1 + \theta_T^d)(\epsilon_p - (0.09 - 0.06\theta_T^d))] \tag{32}$$

Fig. 6 shows the evolution of the different contributions to the yield strength of the material evaluated in Eq. 17 for a distribution of n_f indicated by curve I in Figure 5. During the deformation process when a fraction n_f of the carbides detach from the matrix, $1 - n_f$ remain to impede dislocations motion and the Orowan bowing contribution σ_y^p is reduced as seen in Eq. 15. Moreover, the more carbides debond the fewer remain to generate dislocation loops for increasing hardening. Therefore σ_y^{Lo} decreases as stated in Eq. 16. When carbides fail they are effectively replaced by pores that contribute to the yield strength, although at a lower level.

The uniaxial material response described in Eq. 25 has been combined with the diffusion equation of Eq. 26 to determine the interaction between the diffusion and plasticity models for a situation where a non-uniform hydrogen concentration profile is developed in a component as shown in Fig. 3. Each location: I, II, III, IV, V,VI in Fig. 7 exhibits a different behaviour. Location I which is at $x = 0$ experiences the highest hydrogen content as seen in Fig. 4. The material hardens as a result of (a) the presence of the particles and (b) increasing plastic strain as more prismatic loops are punched out from the surface of the particles. Carbides then start to decohere from the matrix hence (a) fewer particles remain to obstruct the motion of dislocations and (b) as more particles fail fewer remain to generate dislocation loops to contribute to further hardening. The contributions of (a) and (b) to the softening response is most evident at location I in Fig. 7 as it is the place with the highest hydrogen content and hence the weakest interfaces. Moving away from the source, the number fraction of failed carbides n_f decreases as seen in Fig. 5 as locations II, III, IV, V, VI experience a lower concentration of hydrogen. The material behaviour then gradually improves. The peak stress in Fig. 7 increases from 0.3GPa at location I to about 0.8GPa at location VI. The plastic strain corresponding to the peak stress also increases from 10% to about 17%. The degree of softening decreases due to the fact that the strength of the interface improves with increasing distance from the hydrogen source.

Conclusions

This paper presents a mesoscopic constitutive model for a precipitate strengthen material. Simulations are representative of an area containing fine carbides of an AISI8630/IN625 dissimilar weld in which cracks propagate along the interface between the carbides and surrounding matrix. The model reproduces the effect of hydrogen concentration on the constitutive response at the scale of the interaction between carbides and discrete dislocations. These carbides are considered as (a) strengthening elements if the interface between particles and matrix is intact or (b) weakening elements if the interface fails and the particles are effectively are substituted by voids. The model is capable of reproducing the effects of hydrogen on the behaviour of the carbide-rich area: (a) promoting the development of dislocation structures at the M_7C_3 carbides which increases the stress on the particles; (b) reducing the strength of the carbide-matrix interface. Results of the combination of (a) and (b) show that the regions where the concentration of hydrogen is low will harden

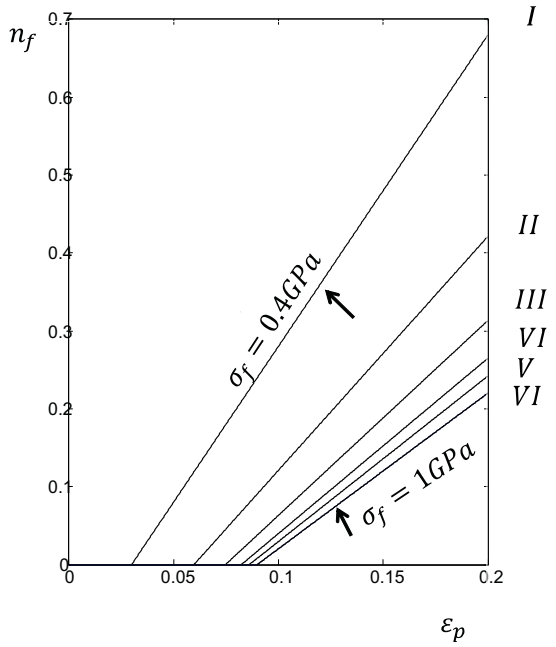

Figure 5: Volumetric fraction of failed carbides n_f as function of plastic strain for different values of critical stress of the interface. Curve (VI) corresponds to $\sigma_f = 1GPa$, curve (I) corresponds to $\sigma_f = 0.4GPa$.

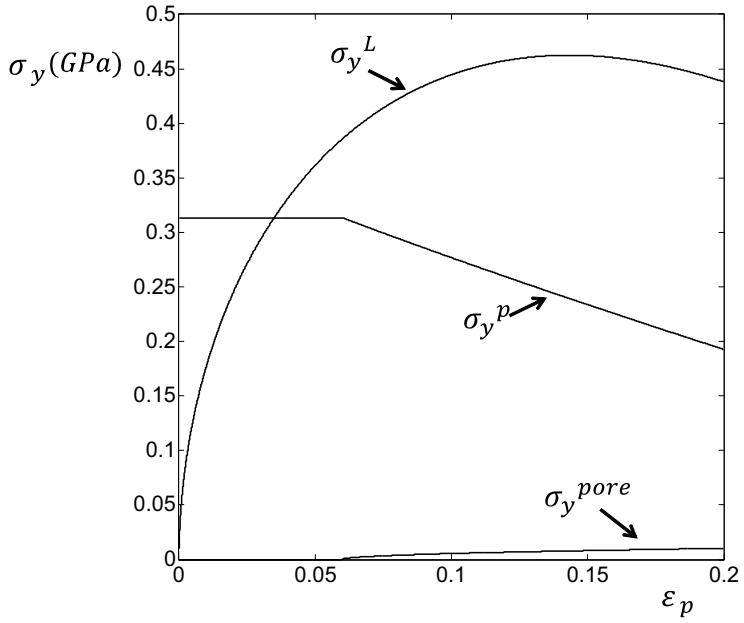

Figure 6: Contributions to the yield stress in Eq. 17: $\sigma_y^p, \sigma_y^L, \sigma_y^{pore}$ at location VI.

as few particles fail and most interfaces remain intact. Locations where the hydrogen concentration is high exhibit softening as a large number of particles fail.

Acknowledgement

This research was supported by the EPSRC through the HEmS Programme Grant EP/LO/4742/1. O.B would like to acknowledge the European Union's Horizon 2020 -EU.1.3.2. - Nurturing excellence by means of cross-border and cross-sector mobility under the Marie Skłodowska-Curie individual fellowship MSCA-IF-2017, MetaBioMec, Grant agreement ID: 796405.

References

[1] V. Olden, P. E. Kvaale, P. A. Simensen, S. Aaldstedt , J. K.Solberg . [1] The Effect of PWHT On The Material Properties And Micro Structure In Inconel 625 And Inconel 725 Buttered Joints. *Cancun, Mexico : OMAE, OMAE 2003-37196*, 2003.

[2] V. C. M. Beaugrand, S. L. Smith, M.F. Gittos. Hydrogen embrittlement of 8630M/625 subsea dissimilar joints: factors that influence the performance. *Proceedings of the 28th International Conference on Ocean, Offshore and Arctic Engineering OMAE2009 Honolulu, Hawaii, USA*, 2009.

[3] M.F. Gittos. [2] Resistance Of Dissimilar Joints Between Steel And Nickel Alloys To Hydrogen-Assisted Cracking. *NACE, NACE 2008-08095.*, 2008.

[4] P. E. Kvaale, Rørvik G. Experience With Qualification And Use of Stainless Steels In Subsea Pipelines. *Vancouver, Canada : 23rd International Conference on Offshore Mechanics and Arctic Engineering, OMAE 2004-5136*, 2004.

[5] M.F. Dodge, H.B. Dong, M. Milititsky, R.P. Barnett, V.F. Marques, M.F. Gittos. Environment-induced cracking in weld joints in subsea oil and gas systems- PART I. *Proceedings of the 31st International Conference on Ocean, Offshore and Arctic Engineering OMAE2012 Rio de Janeiro, Brazil*, 2012.

[6] M.F. Dodge, H.B. Dong, M. Milititsky, R.P. Barnett, V.F. Marques, M.F. Gittos. Environment-induced cracking in weld joints in subsea oil and gas systems- PART II. *Proceedings of the 31st International Conference on Ocean, Offshore and Arctic Engineering OMAE2013 Nantes, France*, 2013.

[7] O. Barrera, A. C. F. Cocks. Computational modelling of hydrogen embrittlement in weld joints of subsea oil and gas component. *Proceedings of the 31st International Conference on Ocean, Offshore and Arctic Engineering OMAE2013 Nantes, France*, 2013.

[8] P. Sofronis, I.M. Robertson. Viable mechanisms of hydrogen embrittlement-a review. *USA: AIP*, 2006.

[9] O. Barrera, A. C. F. Cocks. Computational modelling of hydrogen embrittlement in welded structures. *Phil Mag*, 93:20, 2680-2700, 2013.

[10] O. Barrera, E. Tarleton,A. C. F. Cocks. A micromechanical image-based model for the featureless zone of a Fe–Ni dissimilar weld. *Phil Mag*, 94, 1361-1377, 2014.

[11] I. Robertson The effect of hydrogen on dislocation dynamics. *Engineering Fracture Mechanics*, 64, 649-673, 1999

[12] H. Kitaguchi, S. Lozano-Perez Private communications.

[13] M.F. Ashby. The theory of the critical shear stress and work hardening of dispersion-hardened crystal. *Strengthening Methods in crystals, edited by A. Kelly and R.B. Nicholson, Elsevier, Chap. 3*, 1971.

[14] M.F. Ashby. The deformation of plastically non-homogeneous materials. *Phil Mag*,21:170, 399-424, 1969.

[15] J.J. Gilman Micromechanics of flow in solids. *New York : McGraw-Hill*, 1969.

[16] Y. Dong, T. Nogaret, W.A. Curtin Scaling of dislocation strengthening by multiple obstacle types. *Met and Mat Trans.A*, 41, 2010.

[17] R.C. Picu, R.Li, Z.Xu Strain rate sensitivity of thermally activated dislocation motion across fields of obstacles of different kind. *Materials Science and Engineering A*, 502, 164-171, 2010.

[18] L.M. Brown Toward a sound understanding of dislocation plasticity. *Met. Trans. A*, 22A, 1693-1708, 1991.

[19] L.M. Brown and D.R. Clarke Work hardening due to internal stresses in composite materials. *Acta Metal.*, 23, 821-830, 1975.

[20] A. McNabb and P.K. Foster A new analysis of the diffusion of hydrogen in iron and ferritic steels. *Journal of Transaction of the Metallurgical Society of AIME*, 227, 618-627, 1963.

[21] R.A. Oriani Hydrogen embrittlement of steels. *Annual reviews in Materials Science*, 8:327–357, 1978.

[22] P. Sofronis and R.M. McMeeking Numerical analysis of hydrogen transport near a blunting crack tip. *J. Mech. Phys. Solids*, 37:317–350, 1989.

[23] A.H.M. Krom, R.W.J. Koers and A. Bakker Hydrogen transport near a blunting crack tip. *J. Mech. Phys. Solids*, 47:971–992, 1999.

[24] A.H.M. Krom and A. Bakker Hydrogen trapping models in steel. *Met. and Mat. trans.B*, 31B:1475–1482, 2000.

[25] A.J. Kumnick and H.H. Johnson Deep trapping states for hydrogen in deformed iron. *Acta Met.*, 28:33–39, 1979.

[26] G.M. Pressouyre. Trap theory of hydrogen embrittlement. *Acta Metall.*, 28:895–911, 1980.

[27] P. Novak, R. Yuan, B. P. Somerday, P. Sofronis, and R. O. Ritchie. A Statistical, Physical-based, Micro-mechanical Model of Hydrogen-induced intergranular fracture in Steel. *Journal Mech. Phys. Solids*, 58, 206-226, 2010.

[28] M. Dodge, M. Milititsky Private communications.

[29] Y. Liang and P. Sofronis. Toward a Phenomenological Description of Hydrogen-Induced Decohesion at Particle/Matrix Interfaces. *Journal of Mechanics and Physics of Solids*,51, 1509-1531, 2003.
[30] Jianan Hu, Bo Chen, David J. Smith, Peter E.J. Flewitt, and Alan C.F. Cocks On the evaluation of the Bauschinger effect in an austenitic stainless steel—The role of multi-scale residual stresses. *International Journal of Plasticity*, 84:203–223, 2016.
[31] O. Barrera, E. Tarleton, H.W. Tang and A.C.F. Cocks Modelling the coupling between hydrogen diffusion and the mechanical behaviour of metals. *Computational Materials Science*, 122:219–228, 2016.
[32] Barrera, O., Bombac, D., Chen, Y. et al. Understanding and mitigating hydrogen embrittlement of steels: a review of experimental, modelling and design progress from atomistic to continuum. *J Mater Sci 53, 6251–6290*, 2018.
[33] E. Elmukashf, E. Tarleton, and A.C.F. Cocks A modelling framework for coupled hydrogen diffusion and mechanical behaviour of engineering components. *Computational mechanics*, in press, 2020.
[34] C.D. Beachen A new model for hydrogen-assisted cracking (hydrogen "Embrittlement"). *Matallurgical transactions*, 3: 437-451, 1971.
[35] H. K. Birnbaum and P. Sofronis. Hydrogen Enhanced Localized Plasticity Mechanism for Hydrogen Related Fracture. *Materials Science and Engineering*, A176, 191-202, 1994.
[36] Fernández-Sousa, Rebeca and Betegón, Covadonga and Martínez-Pañeda, Emilio Analysis of the influence of microstructural traps on hydrogen assisted fatigue Acta Materialia,199,253–263, 2020

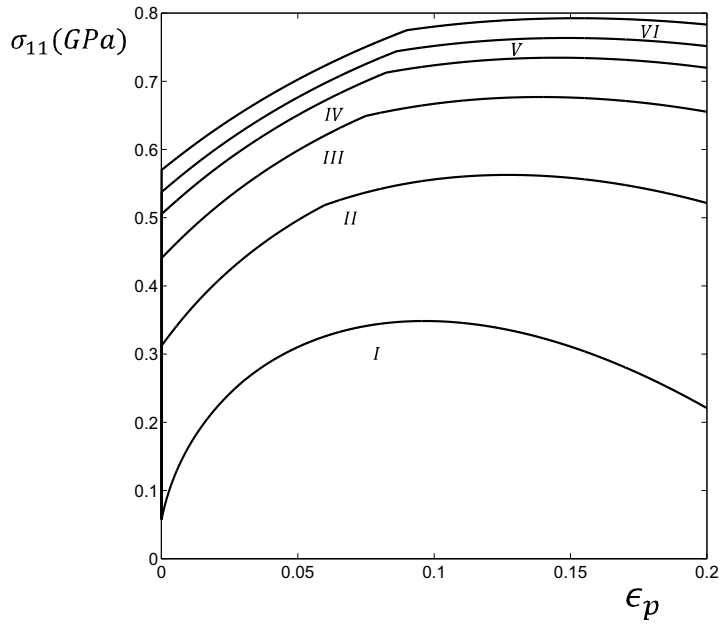

Figure 7: Uniaxial stress-strain response at different locations along x in Fig. 3 .